

Estimation of the leaf area density distribution of individual trees using high-resolution and multi-return airborne LiDAR data

Haruki Oshio^{a,*}, Takashi Asawa^b, Akira Hoyano^c and Satoshi Miyasaka^d

^a Department of Environmental Science and Technology, Tokyo Institute of Technology, JSPS Research Fellow DC, 4259-G5-2, Nagatsuta-cho, Midori-ku, Yokohama, Kanagawa, 226-8502, Japan, oshio.h.aa@m.titech.ac.jp

^b Department of Environmental Science and Technology, Tokyo Institute of Technology, 4259-G5-2, Nagatsuta-cho, Midori-ku, Yokohama, Kanagawa, 226-8502, Japan, asawa.t.aa@m.titech.ac.jp

^c The Open University of Japan, 2-11, Wakaba, Mihama-ku, Chiba, 261-8586, Japan, hoyano@ouj.ac.jp

^d Nakanihon Air Service CO., LTD., 17-1, Toyobawakamiya, Toyoyama-cho, Nishikasugai, Aichi, 480-0202, Japan, miyasaka@nnk.co.jp

* Corresponding author. Tel.: +81 459245510; Fax: +81 459245553. E-mail address: oshio.h.aa@m.titech.ac.jp (Haruki Oshio). Postal address: 4259-G5-2, Nagatsuta-cho, Midori-ku, Yokohama, Kanagawa, 226-8502, Japan

ABSTRACT

The three-dimensional structures of individual trees are important pieces of information necessary to understand the effect of trees on urban environments. In this study, we demonstrate a method for estimating the leaf area density (LAD) distribution of individual trees using high-resolution airborne LiDAR. This method improves upon the previously proposed method, which calculates LAD based on the contact frequency between the laser beams and leaves by tracing the paths of the laser beams. The proposed method in this study exploits the last and intermediate pulses in addition to the first and single pulses to capture the foliage distribution in the inner part of the crown. Each laser beam is traced from a point derived by the last pulse to the point derived by the first or intermediate pulse that is recorded immediately before the last pulse. The laser beam interceptions and intersections can thus be accurately reproduced while considering the last and intermediate pulses. We verify the estimation accuracy of the three-dimensional LAD distribution using terrestrial LiDAR data from a single tree (*Z. serrata*). The appropriate voxel size for representing the LAD distribution from the airborne LiDAR is first determined by comparing the distribution of voxels containing one or more airborne LiDAR points with that containing one or more terrestrial LiDAR points. The estimated LAD distribution with a voxel size of $1\text{ m} \times 1\text{ m} \times 0.5\text{ m}$ is subsequently compared to the terrestrial LiDAR-derived LAD distribution. When only the first and single pulses are used, the LAD is overestimated and underestimated in the upper and

lower part of the crown, respectively. We confirmed that using the last and intermediate pulses improves the estimation accuracy of the entire crown area.

Keywords: leaf area density (LAD), airborne LiDAR, terrestrial LiDAR, tree

1. Introduction

Trees in urban spaces have a significant influence on urban environments through solar shading, transpiration, windbreak, air purification and soundproofing. Knowledge of the three-dimensional structures of individual trees is important for their maintenance and understanding their effects on urban environments. The leaf area density (LAD) distribution is a key index for characterizing the vertical and horizontal crown structure and is defined as the total one-sided leaf area per unit volume.

Various ground-based indirect methods for measuring LAD distribution have been studied. The point quadrat method (Wilson, 1960; Wilson, 1963) offers an accurate estimation when sufficient probes are inserted into the target canopy. A three-dimensional light transfer model based on the point quadrat method, which can estimate the photosynthetic photon flux density distribution in a crown with high accuracy, has been developed (Iio et al., 2011). However, the point quadrat method is notably laborious. The gap fraction method, which measures transmitted light under the

target canopy, is often used to capture foliage density. In particular, a LAI-2000 (LI-COR) plant canopy analyzer (Welles & Norman, 1991) has been employed in many studies to obtain the leaf area index (LAI). Although techniques for estimating the influence of leaf clumping have been studied (Chen et al., 1997; Ryu et al., 2010), three-dimensional foliage distribution is difficult to measure. Recently, terrestrial light detection and ranging (LiDAR) has received significant attention as a means of determining the canopy structure. Detailed tree models, which reconstruct each shoot or leaf, have been generated (Côté et al., 2009; Côté et al., 2011; Hosoi et al., 2011). High-resolution terrestrial LiDAR observation offers an accurate estimation of the LAD distribution (Hosoi & Omasa, 2006; Hosoi & Omasa, 2007). However, it is laborious to measure many trees on the ground.

Airborne small-footprint LiDAR can acquire three-dimensional information of many trees with a high spatial resolution in a short amount of time. The following methods for deriving the tree geometry from airborne LiDAR data have been well-researched: tree height (Omasa et al., 2000; Hyypä et al., 2001; Næsset & Økland, 2002; Persson et al., 2002), crown base height (Holmgren & Persson, 2004; Popescu & Zhao, 2008) and crown shape and volume (Omasa et al., 2008; Hecht et al., 2008; Kato et al., 2009). LAI estimation has also been investigated using gap fractions (Solberg et al., 2009; Korhonen et al., 2011), regression models of LiDAR metrics (Riaño et al., 2004; Farid et al., 2008; Jensen et al., 2008; Zhao and Popescu, 2009) and the contact frequency

between laser beams and foliage (Morsdorf et al., 2006). Wang et al. (2008) and Sasaki et al. (2012) also attempted a voxel-based reproduction of the foliage distribution. However, these researchers did not consider the LAD for each voxel.

Methods for estimating LAD distribution using airborne LiDAR have been explored less thoroughly. Hosoi et al. (2011) developed a method for estimating LAD distribution by combining airborne and terrestrial LiDAR. These authors calculated the LAD based on the contact frequency between the laser beams and the leaves. The contact frequency was computed by tracing the path of the laser beams and counting the laser beam interceptions and intersections in each layer. These researchers used an airborne LiDAR point cloud acquired by the first pulse mode, yielding an underestimated LAD when only airborne data were used. Song et al. (2011) proposed a method for estimating PAD distribution involving the acquisition of airborne LiDAR data by employing a multi-pulse mode. However, laser beams were traced from the points derived by only the first or single pulses to avoid the multiple counting of one laser beam.

The objective of our research is to develop a method of estimating the LAD distribution of individual trees by exploiting the last and intermediate pulses in addition to the first and single pulses using high-resolution airborne LiDAR. The LAD distribution of a single tree derived from terrestrial LiDAR was used to verify the estimation accuracy. An appropriate voxel size for representing the LAD distribution by the airborne LiDAR data was first determined. The accuracy

of the estimated LAD and the influence of the utilization of the last and intermediate pulses were subsequently analyzed.

2. Materials

2.1 Airborne LiDAR data

The study site used was Hisaya-Odori Street in Nagoya, Japan. Hisaya-Odori Street is broad and lined with numerous broadleaved trees. A helicopter-based laser scanning system (Nakanihon Air Service) with a LMS-Q560 sensor (RIEGL) was employed for the airborne LiDAR observation. Fig. 1 shows the flight run, and Table 1 shows the data acquisition specifications. The flight altitude was 350 m. The footprint diameter was 0.18 m, and the distance between the consecutive footprint centers was 0.2 m (flight direction) and 0.25 m (scan direction) on the ground under the flight run. Multi-pulse mode was used; first, intermediate, last and single pulses were obtained. The number of return pulses per one laser shot that the sensor could obtain was unlimited. Airborne LiDAR data were acquired on September 6, 2010, which is summer in Japan. Fig. 2 (left) shows the airborne LiDAR data of the study site. A Japanese Zelkova (*Z. serrata*) tree was selected for analysis. Fig. 1 shows the location of the tree. The tree height is 10.5 m, the average crown diameter is 8.5 m and the crown length is 7 m. Fig. 2 (right) shows the airborne LiDAR point cloud of the tree. The characteristics of the airborne laser beam transmittance of the selected *Z. serrata* tree are

shown in Fig. 3 (gray line). The ratio of the number of incident laser beams on a bin of height 1 m to the incident on the top bin is plotted against twenty *Z. serrata* trees in the study site. The average height of the twenty trees is 11.5 m with a standard deviation of 1.3 m. The average laser beam transmittance (ratio of the number of return pulses triggered on the ground to that of incident laser beams on the tree) is 0.34. We selected a tree the laser beam transmittance of which is close to the average value for the analysis.

2.2 Field data acquisition and processing

Field measurement was carried out on September 2, 2010. We employed terrestrial LiDAR to obtain the LAD distribution to verify the results derived from the airborne LiDAR. The selected *Z.serrata* tree was measured from two scanning positions using a terrestrial laser scanner (VZ-400; RIEGL) (Fig. 1). The distance between the scanner and the trunk was 10 m. Table 2 shows the measurement specifications. The increments of the zenith and azimuth angles of the laser beam emission were 0.04° , thereby yielding a laser beam interval of 7 mm on a vertical plane 10 m ahead. The shape of a leaf can be recognized from the terrestrial LiDAR point cloud (Fig. 4).

The LAD distribution of the tree was calculated using the terrestrial LiDAR data based on the previously developed method (Hosoi & Omasa, 2006). The parameters for calculating LAD are the contact frequency between the laser beams and the leaves, the zenith angle of the incident laser beam and the mean projection area of a unit leaf area on a plane perpendicular to the laser beam.

The point cloud of the *Z. serrate* tree was divided into $5\text{ mm} \times 5\text{ mm} \times 5\text{ mm}$ voxels (s-voxel-t), which is the same setting as the previous research that measured the *Z. serrata* canopy 9 - 24 m from the center of the canopy (Hosoi & Omasa, 2007). The laser beams were traced using these s-voxel-t, and the contact frequency was calculated. The zenith angle of the incident laser beam was also acquired by the laser beam tracing. The mean projection area of a unit leaf area was calculated using the inclination angles of the leaves in each voxel. The leaf inclination angle was given based on the field measurement data of the roadside trees of *Z. serrate* in Japan, as reported by Simojo et al. (2006). The average angle obtained from the upper and lower parts of the crowns was used in all voxels.

Although terrestrial LiADR is an effective method for capturing LAD distribution, voxels where the terrestrial laser beam incident condition is fine were selected to achieve an accurate verification. We used voxels with a terrestrial laser beam incident ratio (TLIR) greater than 0.8 to verify the airborne LiDAR-derived LAD. The TLIR is given by N_a/N_t , where N_a is the number of incident terrestrial laser beams on a voxel and N_t is the number of incident terrestrial laser beams on a voxel if no laser beams are intercepted by the objects between the voxel and the scanner. This type of approach has been used to evaluate laser beam interceptions before reaching the voxel (Durrieu et al., 2008; Béland et al., 2011). Voxels that were occupied by branches were manually detected.

3. Methods

3.1 Analysis of the spatial resolution of the information derived from airborne LiDAR

If there are many unextracted voxels from airborne LiDAR, the crown is not represented by the voxels. We define an unextracted voxel as a voxel that contains no airborne LiDAR points and contains one or more terrestrial LiDAR points. Therefore, before estimating the LAD distribution, we examined the appropriate voxel size for the airborne LiDAR data to reduce the unextracted voxels. The airborne LiDAR point cloud of the selected *Z. serrate* tree was divided into voxels. Three different voxel sizes were used: $0.5\text{ m} \times 0.5\text{ m} \times 0.5\text{ m}$, $0.75\text{ m} \times 0.75\text{ m} \times 0.5\text{ m}$ and $1\text{ m} \times 1\text{ m} \times 0.5$. Voxels containing one or more airborne LiDAR points were extracted in areas in which leaves were distributed. Voxels were also extracted from terrestrial LiDAR data in the same way as airborne LiDAR. First, the extraction ratio was calculated. The extraction ratio is expressed as $N_{air \cap ter}/N_{ter}$, where $N_{air \cap ter}$ is the number of voxels extracted by airborne and terrestrial LiDAR and N_{ter} is the number of voxels extracted by terrestrial LiDAR.

Voxels with low LAD values are difficult to extract using airborne LiDAR. However, the influence on the reproduction of the crown is small even if such low LAD voxels are not extracted. Unextracted voxels are then classified into two categories: the voxel contains insufficient leaves to trigger a return pulse that the sensor can recognize (Voxel A), and there are no incident laser beams on the leaves in the voxel, even if the voxel contains more leaves than Voxel A (Voxel B).

Fig. 5 shows the procedure for the classification. Terrestrial LiDAR-derived LAD was used to distinguish between Voxel A and Voxel B. First, voxels with a TLIR less than 0.8 were removed from the analysis (Voxel C, Fig. 5 Step 1). The threshold in Step 2 was calculated using voxels where there were no objects between the voxel and the airborne LiDAR scanner. The maximum terrestrial LiDAR-derived LAD value of the voxels containing no airborne LiDAR points was employed for the threshold. If the LAD of an unextracted voxel is less than the threshold, the voxel is considered to contain insufficient leaves to trigger a return pulse (Voxel A). If one of the adjacent voxels of an unextracted voxel is extracted, the error is within one voxel. In particular, the influence of the unextracted voxel on the reproduction of the crown is small when the unextracted voxel is Voxel A. Therefore, Voxel A, Voxel B and Voxel C were further classified whether at least one of the adjacent voxels was extracted by the airborne LiDAR.

3.2 Estimating LAD distribution using airborne LiDAR data

The LAD for each voxel was calculated based on the contact frequency between the airborne laser beams and the leaves using the same equation as in the previously developed method (Hosoi & Omasa, (2006)).

$$LAD = \frac{1}{\Delta H} \cdot \frac{\cos(\theta)}{G(\theta)} \sum_{k=1}^N \frac{n_i(k)}{n_i(k) + n_p(k)} \quad (1)$$

where ΔH is the height of the voxel, θ is the incident laser beam zenith angle, $G(\theta)$ is the mean

projection area of a unit leaf area on a plane perpendicular to the laser beam, N is the number of layers in a voxel, $n_i(k)$ is the number of laser beam interceptions in the k th layer and $n_p(k)$ is the number of laser beam intersections in the k th layer.

Hosoi et al. (2011) calculated $n_i(k)$ and $n_p(k)$ as follows: the airborne LiDAR point cloud of the target canopy is divided into voxels (s-voxel-a), the size of which are comparable to the airborne LiDAR spatial resolution. $n_i(k)$ is given by the number of s-voxel-a containing one or more airborne LiDAR points in the k th layer. $n_p(k)$ is the number of s-voxel-a that were intersected by one or more laser beams in the k th layer. These voxels are detected by tracing the path of the laser beams. In this tracing, there is a possibility that a ray does not hit a voxel containing a point, although the ray is representing the laser beam that causes a reflection pulse. Therefore, the precise reproduction of the laser beam interceptions and intersections, including the last and intermediate pulses, is difficult. Song et al. (2011) estimated the PAD distribution using the same principle as that of equation (1). They traced each laser beam between the point derived by the first or single pulse and the airborne LiDAR scanner using flight line information. Laser beam interceptions and intersections were counted in each voxel. The last and intermediate pulses were excluded to avoid the multiple counting of one laser beam. Furthermore, these researchers assumed that the flight line was perpendicular to the scan line. However, the airframe is not parallel to the flight direction, and the flying posture also depends on wind conditions; a precise trace of the path of the laser

beams is difficult to achieve.

Fig. 6 shows a schematic diagram of the proposed method in this study. Each voxel is divided into several layers, and $n_i(k)$ and $n_p(k)$ in equation (1) are calculated in each layer. $n_i(k)$ is given by the number of points in the layer. $n_p(k)$ is calculated through laser beam tracing as follows: for the points derived by the last or intermediate pulses, each laser beam is traced from that point to the point derived by the first or intermediate pulse that was recorded just before the last or intermediate pulse. The tracing direction is precisely determined. Because multiple return pulses to one laser beam are recorded in succession, the accurate position of the point that was recorded before or after the target point can be detected. For the points derived by first or single pulses, each laser beam is traced from the point to the sky. The direction of the tracing was determined as follows: for the points derived by the first pulses, the last or intermediate pulse that was recorded just after the first pulse is used. For the points derived by single pulses, the average direction of the tracing for the first pulses is used. The last and intermediate pulses can easily be included in the calculation without missing tracing. No information is needed regarding the flight line or the position and direction of the laser beam emission. Although more investigations into the appropriate thickness layer are required, we selected a thickness layer of 0.1 m in the same way as the previous study (Hosoi et al., 2011). The height of the voxel was 0.5 m (3.1), yielding five layers in the voxel.

4. Results and Discussion

4.1 Distribution of voxels used in the LAD verification

Voxels for the fine terrestrial incident laser beam condition were selected for an accurate verification of the airborne LiDAR-derived LAD. We employed voxels with a TLIR greater than 0.8. Fig. 7 (left) shows the distribution of TLIR when the voxel size is $1\text{ m} \times 1\text{ m} \times 0.5\text{ m}$. The employed voxels distribute in the lower part of the crown and the periphery. Fig. 7 (right) shows the vertical distribution of the ratio of voxels with a TLIR greater than 0.8 to all voxels at each height. The ratio is 20 to 30 % in the upper part of the crown. However, the difference in the conditions of the airborne incidence laser beam is small among the voxels in the upper part. The difference becomes large toward the lower part, but the ratio in Fig. 7 reaches 88 % in the lower four layers. Therefore, we decided that the airborne LiDAR-derived LAD in the upper part and lower part can be verified by the terrestrial LiDAR data. The foliage density of the used *Z. serrata* tree was intermediate. Therefore, considering the results of Hosoi et al., the LAD was well-calculated by terrestrial LiDAR in the area where the terrestrial incident laser beam condition was fine. However, further research is required for the terrestrial LiDAR-based LAD estimation of dense trees where most of the terrestrial laser beams are intercepted in each voxel.

4.2 Comparison between airborne LiDAR-derived and terrestrial LiDAR-derived voxel distribution

Unlike the observation with the high laser beam density by terrestrial LiDAR, voxel size is important for airborne LiDAR-based estimation because the spatial resolution is on a 0.1-m scale. Therefore, the appropriate voxel size for the airborne LiDAR-based LAD estimation is examined. Fig. 8 (1) shows the three-dimensional distribution of the voxels. Two different voxel sizes are presented. Fig. 8 (2) shows the horizontal sections of the three-dimensional voxel distribution at the upper and lower part of the crown. The depth of the section is 0.5 m. As the figure indicates, the distribution of voxels derived from the airborne LiDAR data matches the distribution derived from the terrestrial LiDAR data for the upper part of the crown with a voxel size of $1\text{ m} \times 1\text{ m} \times 0.5\text{ m}$. On the other hand, in the case of a $0.5\text{ m} \times 0.5\text{ m} \times 0.5\text{ m}$ voxel, there are many voxels that are not extracted by airborne LiDAR but extracted by terrestrial LiDAR, even in the upper part of the crown.

A quantitative accuracy evaluation was then performed based on the extraction ratio. Fig. 9 shows the vertical distribution of the extraction ratio according to height. Although there were many incident laser beams on the voxels in the upper part of the crown, the extraction ratio is 40 - 60 % for a voxel size of $0.5\text{ m} \times 0.5\text{ m} \times 0.5\text{ m}$ because the voxel contained an insufficient amount of leaves to trigger a return pulse that the sensor can recognize. The extraction ratio decreases to less than 40 % in the lower part of the crown. The number of voxels in which there were no airborne incident laser beams on the leaves is expected to increase toward the lower part of the crown. The

difference in the extraction ratio between a voxel size of $0.75 \text{ m} \times 0.75 \text{ m} \times 0.5 \text{ m}$ and $1 \text{ m} \times 1 \text{ m} \times 0.5 \text{ m}$ is minimal in the four layers from the treetop. However, the difference increases toward the lower part of the crown, reaching 20 %. Table 3 shows the extraction ratio in the entire crown area. The extraction ratio is 44.2 % for a voxel size of $0.5 \text{ m} \times 0.5 \text{ m} \times 0.5 \text{ m}$. When the voxel size is $1 \text{ m} \times 1 \text{ m} \times 0.5 \text{ m}$, the extraction ratio is 69.3 %. The extraction accuracy is thus relatively low for a voxel size of $0.5 \text{ m} \times 0.5 \text{ m} \times 0.5 \text{ m}$ and $0.75 \text{ m} \times 0.75 \text{ m} \times 0.5 \text{ m}$; thus, we employed a voxel size of $1 \text{ m} \times 1 \text{ m} \times 0.5 \text{ m}$. The reasoning behind the unextracted voxels (i.e., voxels not being extracted by airborne LiDAR) is analyzed in the next section.

4.3 Characteristics of unextracted voxels

First, the threshold of the terrestrial LiDAR-derived LAD for classifying the unextracted voxels into Voxel A and Voxel B (Fig. 5, Step 2) is examined. Fig. 10 shows the frequency distribution of the terrestrial LiDAR-derived LAD for the voxels where there were no objects between the voxel and the airborne LiDAR scanner. The threshold is the maximum terrestrial LiDAR-derived LAD value of the voxels not extracted by the airborne LiDAR; the threshold is $0.064 \text{ m}^2/\text{m}^3$. If the terrestrial LiDAR-derived LAD is less than the threshold, the unextracted voxel is expected to contain an insufficient amount of leaves to trigger a return pulse (Voxel A). The influence of Voxel A on the reproduction of the LAD distribution is minimal.

Next, unextracted voxel classification is examined. Fig. 11 shows the breakdown of unextracted

voxels according to height. The number of Voxel A (i.e., the voxel containing an insufficient amount of leaves to trigger a return pulse) is greater than that of Voxel B (i.e., there were no incident laser beams on the leaves) in the upper half of the crown. There are some Voxel C (i.e. where the TLIR is less than 0.8) in this area. However, the main cause of these unextracted voxels is considered to be the voxels containing an insufficient amount of leaves necessary to trigger a return pulse as Voxel A. In this area, all unextracted voxels are voxels at least one adjacent voxel of which was extracted by the airborne LiDAR. Therefore, the influence of the unextracted voxels on the reproductivity of the foliage distribution is minimal. The number of Voxel B increases toward the lower part of the crown. However, most of the Voxel B is a voxel at least one adjacent voxel of which is extracted.

The ratio of the number of extracted voxels and Voxel A at least one adjacent voxel of which was extracted (■ + ■) to the number of all voxels except Voxel C (■ + ■ + ■ + ■ with black frame + ■ with black frame) is 85.6 % for the entire crown area. If we see the upper and middle parts of the crown, which have a large influence on the light absorption and transmission by the crown, the ratio is 95.2 % in the 2 - 7 m height range from the crown base. We therefore conclude that the LAD distribution can be represented by the voxels with a size of 1 m × 1 m × 0.5 m.

4.4 LAD distribution derived from airborne LiDAR

Fig. 12 shows scatter plots of airborne LiDAR-derived LAD and terrestrial LiDAR-derived LAD.

Each cross and circle indicates the result of a $1\text{ m} \times 1\text{ m} \times 0.5\text{ m}$ voxel. Used return pulse types in the airborne LiDAR estimation are different among (1) – (3). The black cross indicates voxels in the upper half of the crown, and the gray circle indicates voxels in the lower half of the crown. Fig. 12 (1) displays the results derived from the first and single pulses. In this case, the calculation method is the same as our method, but the used pulse is the same as in previous studies (Hosoi et al., 2011; Song et al., 2011). The airborne LiDAR-derived LAD is strongly correlated with the terrestrial LiDAR-derived LAD in the upper half of the crown ($R^2 = 0.87$). However, the LAD is overestimated in most voxels because the laser beam intersections are underestimated, as the laser beams between the first and last or intermediate pulses were not counted. The mean ΔLAD ($=|\text{Airborne LiDAR-derived LAD} - \text{Terrestrial LiDAR-derived LAD}|$) is $0.19\text{ m}^2/\text{m}^3$. On the other hand, the LAD is estimated as 0 for most voxels in the lower half of the crown, as these voxels contained no airborne LiDAR points derived by first or single pulses. As a result, the mean ΔLAD is $0.35\text{ m}^2/\text{m}^3$ with a R^2 of 0.28 for the entire crown area.

Next, the validity of the proposed method in this study is examined. Fig. 12 (2) shows the result derived from the first, single and last pulses. In the upper half of the crown, the estimation is improved; most points become close to the 1:1 line. The mean ΔLAD is $0.13\text{ m}^2/\text{m}^3$ with a R^2 of 0.84. In the lower half of the crown, the points are scattered, and the LAD is underestimated for most voxels. However, the ΔLAD and R^2 values for the entire crown area are improved (the mean

ΔLAD is $0.27 \text{ m}^2/\text{m}^3$ with a R^2 of 0.33 in the entire crown area). Fig. 12 (3) shows the result derived from the first, single, last and intermediate pulses. In the upper half of the crown, there is almost no change in the result of (2) (the mean ΔLAD is $0.13 \text{ m}^2/\text{m}^3$ with a R^2 of 0.85) because these voxels contain few intermediate pulses. On the other hand, the ΔLAD is $0.23 \text{ m}^2/\text{m}^3$ with a R^2 of 0.47 for the entire crown area. In particular, the correlation is improved by using the intermediate pulses. From the above, the validity of the proposed method, which utilizes the last and intermediate pulses in addition to the first and single pulses, is confirmed.

In the upper part of the crown, the LAD is still overestimated in the low LAD area. The overestimation is expected because we added 1 to $n_i(k)$ in equation (1) for a first pulse although the laser beam footprint of a first pulse is not fully occupied by the leaves. The ratio of the leaf area to a footprint decreases as the LAD become smaller. Thus, a LAD estimation taking into consideration the reflection intensity will be investigated in future studies. In the lower part of the crown, the LAD is still underestimated for most voxels and overestimated for a few voxels because the leaves are not uniformly distributed in the crown. The balance of underestimation and overestimation is expected to vary according to the crown structure. Additional work is required to assess the balance for trees with different structures.

Hosoi et al. (2011) proposed a laser beam coverage index Ω , which represents the area covered by incident laser beams in each layer taking into consideration the laser beam attenuation and

LiDAR's laser beam settings. Ω estimated LAD estimation error well for both terrestrial and airborne LiDAR. However, the area covered by the laser beam footprint is difficult to determine for the last and intermediate pulses. In addition, two laser beams with a footprint area of 1 are expected to offer better LAD estimation than one laser beam with a footprint area of 2. Thus, the number of incident laser beams on each voxel (N) is important. Therefore, we used the airborne N to explain the LAD estimation error. Fig. 13 shows the relationship between the airborne N and ΔLAD in the voxel. The ΔLAD value derived from the first, single, last and intermediate pulses (Fig. 12 (3)) was used. The ΔLAD value was averaged for each airborne N class; this value decreases to $0.2 \text{ m}^2/\text{m}^3$ at an airborne N of 8-11 and varies slightly at larger N values. The estimation accuracy for other *Z. serrate* trees or other types of broad-leaved trees can be assessed by analyzing the distribution of airborne N . Further research is needed to apply these results to trees with different structures.

5. Conclusions

We proposed an airborne LiDAR-based method for estimating the LAD distribution of individual trees, which can precisely compute the laser beam interceptions and intersections, including the last and intermediate pulses. The LAD distribution of a *Z. serrata* tree derived from terrestrial LiDAR was used to verify the estimation accuracy. The appropriate voxel size for the airborne

LiDAR data was first investigated. There were many $0.5\text{ m} \times 0.5\text{ m} \times 0.5\text{ m}$ voxels that contained no airborne LiDAR points even if the voxels were extracted by the terrestrial LiDAR. A total of 69.3 % of the foliage voxels was extracted by the airborne LiDAR when the voxel size was $1\text{ m} \times 1\text{ m} \times 0.5\text{ m}$. Moreover, most of the unextracted voxels contained only a few leaves that was insufficient to trigger a return pulse. The influence of these unextracted voxels on the reproduction of the LAD distribution is small. We subsequently selected this voxel size to represent the LAD distribution.

When only the first and single pulses were used in the same way as the previous studies, the LAD was overestimated in the upper part of the crown and underestimated in the lower part of the crown. Utilization of the last and intermediate pulses improved the estimation accuracy in the entire crown area. The number of airborne incident laser beams on each voxel was strongly correlated with the estimation error. More than eight incident laser beams on a $1\text{ m} \times 1\text{ m} \times 0.5\text{ m}$ voxel offered a LAD estimation within a $0.2\text{ m}^2/\text{m}^3$ difference of the terrestrial LiDAR-derived LAD. We confirmed the validity of the proposed method for *Z. serrate* tree with an average foliage density. In future studies, the proposed method will be tested on other trees with different foliage densities and crown structures. An LAD estimation taking into consideration the reflection intensity will also be investigated. Voxels occupied by branches were manually detected and removed from analysis in this study. Therefore, the influence of branches will be analyzed using airborne LiDAR

data obtained in the winter.

Acknowledgments

We would like to express gratitude to RIEGL Japan for their assistance with the terrestrial LiDAR observations.

References

- Béland, M., Widlowski, J.-L., Fournier R. A., Côté J.-F., & Verstraete, M. M. (2011). Estimating leaf area distribution in savanna trees from terrestrial LiDAR measurements. *Agricultural and Forest Meteorology*, 151, pp. 1252-1266, 2011.
- Chen, J. M., Rich, P. M., Gower, S. T., Norman, J. M., & Plummer, S. (1997). Leaf area index of boreal forests: Theory, techniques, and measurements. *Journal of Geophysical Research*, 102, 29,429-29,443.
- Côté, J.-F., Widlowski, J.-L., Fournier, R. A., & Verstraete, M. M. (2009). The structural and radiative consistency of three-dimensional tree reconstructions from terrestrial lidar. *Remote Sensing of Environment*, 113, 1067-1081.
- Côté, J.-F., Widlowski, J.-L., Fournier, R. A., & Egli, R. (2011). An architectural model of trees to estimate forest structural attributes using terrestrial lidar. *Environmental Modelling & Software*,

26, 761-777.

Durrieu, S., Allouis, T., Fournier, R., Vega, C., & Albrech, L. (2008). Spatial quantification of vegetation density from terrestrial laser scanner data for characterization of 3D forest structure at plot level. *SilviLaser 2008*, 325-334.

Farida, A., Goodrich, D.C., Bryant, R., & Sorooshian, S. (2008). Using airborne lidar to predict Leaf Area Index in cottonwood trees and refine riparian water-use estimates. *Journal of Arid Environments*, 72, 1-15.

Hecht, R., Meinel, G., & Buchroithner, M. F. (2008). Estimation of urban green volume based on single-pulse lidar data. *IEEE Transactions on Geoscience and Remote Sensing*, 46(11), 3832-3840.

Holmgren, J., & Persson, A. (2004). Identifying species of individual trees using airborne laser scanner. *Remote Sensing of Environment*, 90, 415-423.

Hosoi, F., & Omasa, K. (2006). Voxel-based 3-D modeling of individual trees for estimating leaf area density using high-resolution portable scanning lidar. *IEEE Transactions on Geoscience and Remote Sensing*, 44(12), 3610-3618.

Hosoi, F., & Omasa, K. (2007). Factors contributing to accuracy in the estimation of the woody canopy leaf area density profile using 3D portable lidar imaging. *Journal of Experimental Botany*, 58(12), 3463-3473.

- Hosoi, F., Nakai, Y., & Omasa, K. (2010). Estimation and error analysis of woody canopy leaf area density profiles using 3-D airborne and ground-based scanning lidar remote sensing techniques. *IEEE Transactions on Geoscience and Remote Sensing*, 48(5), 2215-2223.
- Hosoi, F., Nakabayashi, K., & Omasa, K. (2011). 3-D modeling of tomato canopies using a high-resolution portable scanning lidar for extracting structural information. *Sensors*, 11, 2166-2174.
- Hyypä, J., Kelle, O., Lehtikoinen, M., & Inkinen, M. (2001). A segmentation-based method to retrieve stem volume estimates from 3-D tree height models produced by laser scanners. *IEEE Transactions on Geoscience and Remote Sensing*, 39(5), 969-975.
- Iio, A., Kakubari, Y., & Mizunaga, H. (2011). A three-dimensional light transfer model based on the vertical point-quadrant method and Monte-Carlo simulation in a *Fagus crenata* forest canopy on Mount Naeba in Japan. *Agricultural and Forest Meteorology*, 151, 461-479.
- Jensen, J. L.R., Humes, K. S., Vierling, L. A., & Hudak, A. T. (2008). Discrete return lidar-based prediction of leaf area index in two conifer forests. *Remote Sensing of Environment*, 112, 3947-3957.
- Kato, A., Moskal, L.M., Schiess, P., Swanson, M. E., Calhoun, D., & Stuetzle, W. (2009). Capturing tree crown formation through implicit surface reconstruction using airborne lidar data. *Remote Sensing of Environment*, 113, 1148-1162.
- Korhonen, L., Korpela, I., Heiskanen, J., & Maltamo, M. (2011). Airborne discrete-return LIDAR

data in the estimation of vertical canopy cover, angular canopy closure and leaf area index.

Remote Sensing of Environment, 115, 1065-1080.

Morsdorf, F., Kötz, B., Meier, E., Itten, K.I., & Allgöwer, B. (2006). Estimation of LAI and fractional cover from small footprint airborne laser scanning data based on gap fraction. *Remote Sensing of Environment*, 104, 50-61.

Næsset, E., & Økland, T. (2002). Estimating tree height and tree crown properties using airborne scanning laser in a boreal nature reserve. *Remote Sensing of Environment*, 79, 105-115.

Omasa, K., Akiyama, Y., Ishigami, Y., & Yoshimi, K. (2000). 3-D remote sensing of woody canopy heights using a scanning helicopter-borne lidar system with high spatial resolution. *Journal of the Remote Sensing Society of Japan*, 20(4), 394-406.

Omasa, K., Hosoi, F., Uenishi, T. M., Shimizu, Y., & Akiyama, Y. (2008). Three-dimensional modeling of an urban park and trees by combined airborne and portable on-ground scanning lidar remote sensing. *Environmental Modeling and Assessment*, 13, 473-481.

Persson, A., Holmgren, J., & Soderman, U. (2002). Detecting and measuring individual trees using an airborne laser scanner. *Photogrammetric Engineering & Remote Sensing*, 68(9), 925-932.

Popescu, S., & Zhao, K. (2008). A voxel-based lidar method for estimating crown base height for deciduous and pine trees. *Remote Sensing of Environment*, 112, 767-781.

Riaño, D., Valladares, F., Condés, S., & Chuvieco, E. (2004). Estimation of leaf area index and

- covered ground from airborne laser scanner (Lidar) in two contrasting forests. *Agricultural and Forest Meteorology*, 124, 269-275.
- Ryu, Y., Nilson, T., Kobayashi, H., Sonnentag, O., Law, B. E., & Baldocchi, D. D. (2010). On the correct estimation of effective leaf area index: Does it reveal information on clumping effects?. *Agricultural and Forest Meteorology*, 150, 463-472.
- Sasaki, T., Imanishi, J., Fukui, W., Tokunaga, F., & Morimoto, Y. (2012). Fine-scale replication and quantitative assessment of forest vertical structure using LiDAR for forest avian habitat characterization. *Forest Science and Technology*, 8(3), 145-153.
- Shimojo, M., Yoshida, S., & Ooka, R. (2003). Study on Relaxation Effect of Road Trees on Hot Thermal Environment in Summer (Part 3) : Field Observations of Optical Length, Leaf Area Density and Characteristics of Solar Incidence on Tree Canopy. *Architectural Institute of Japan conference 2003 Summaries of Technical Papers*, D-1, 609-610.
- Solberg, S., Brunner, A., Hanssen, K. H., Lange, H., Næsset, E., Rautiainen, M., & Stenberg, P. (2009). Mapping LAI in a Norway spruce forest using airborne laser scanning. *Remote Sensing of Environment*, 113, 2317-2327.
- Song, Y., Maki, M., Imanishi, J., & Morimoto, Y. (2011). Voxel-based estimation of plant area density from airborne laser scanner data. *ISPRS Workshop Laser Scanning 2011*, XXXVIII-5/W12, 209-212.

- Wang, Y., Weinacker, H., & Koch, B. (2008). A LiDAR point cloud based procedure for vertical canopy structure analysis and 3D single tree modeling in forest. *Sensors*, 8, 3938-3951.
- Warren Wilson, J. (1960). Inclined point quadrats. *New Phytologist*, 59(1), 1-8.
- Warren Wilson, J. (1963). Estimation of foliage denseness and foliage angle by inclined point Quadrats. *Australian journal of botany*, 11, 95-105.
- Welles, J. M., & Norman, J. M. (1991). Instrument for indirect measurement of canopy architecture. *Agronomy Journal*, 83, 818-825.
- Zhao, K., & Popescu, S. (2009). Lidar-based mapping of leaf area index and its use for validating GLOBCARBON satellite LAI product in a temperate forest of the southern USA. *Remote Sensing of Environment*, 113, 1628-1645.

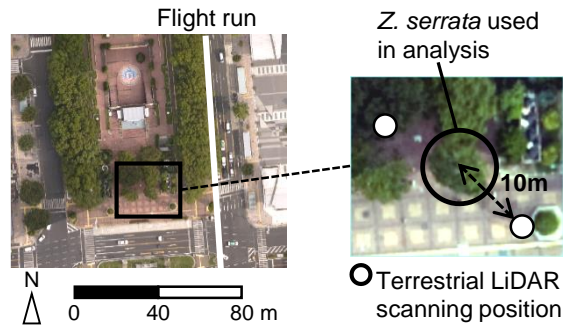


Fig. 1. Airborne LiDAR observation flight run, location of the zelkova tree used in the analysis and terrestrial LiDAR scanning positions.

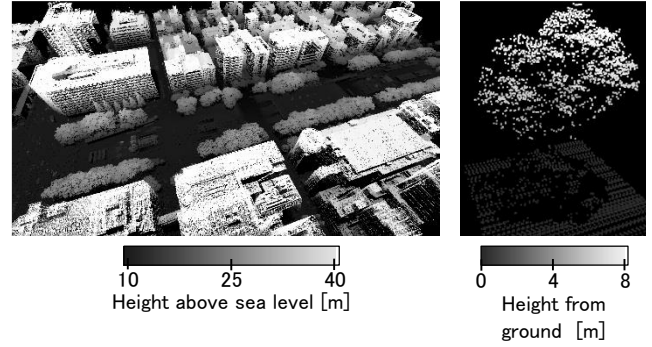


Fig. 2. Airborne LiDAR data (left: Hisata-Odori street, right: *Z. serrata* tree used in the analysis).

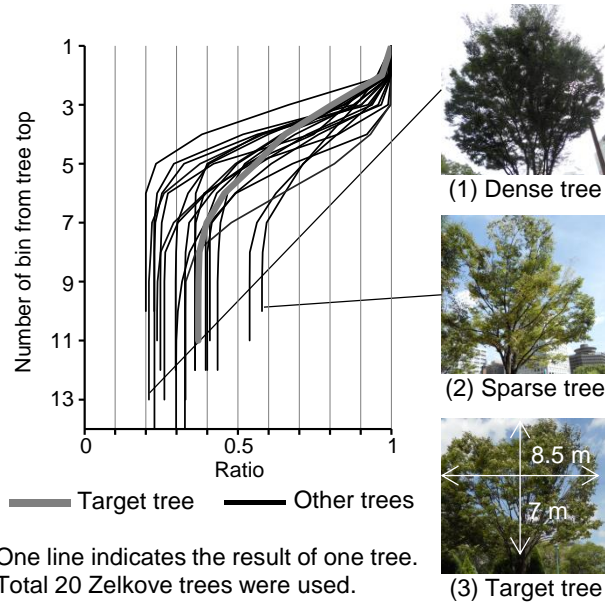


Fig. 3. Ratio of number of incident laser beams on each bin to that on a crown (Height of a bin: 1 m).

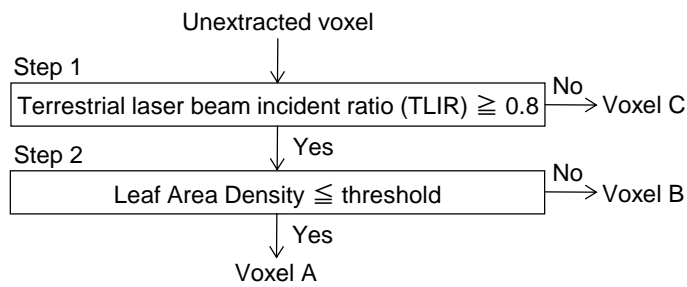


Fig. 5. Procedure of classification of unextracted voxel (voxel containing no airborne LiDAR points but LAD of which is > 0).

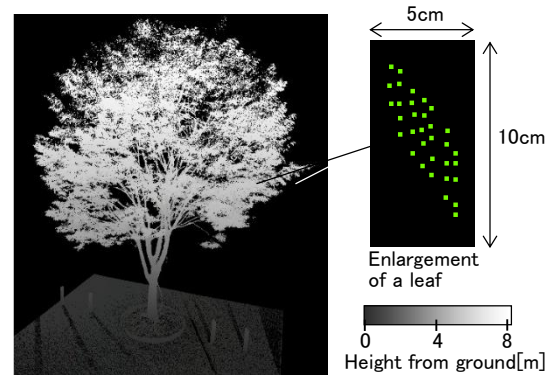


Fig. 4. Terrestrial LiDAR point cloud of the *Z. serrata* tree.

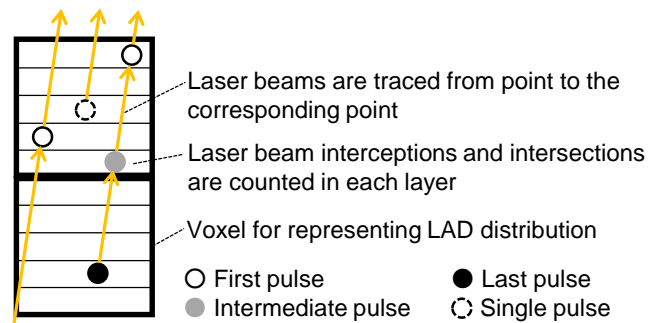


Fig. 6. Schematic diagram of the proposed method.

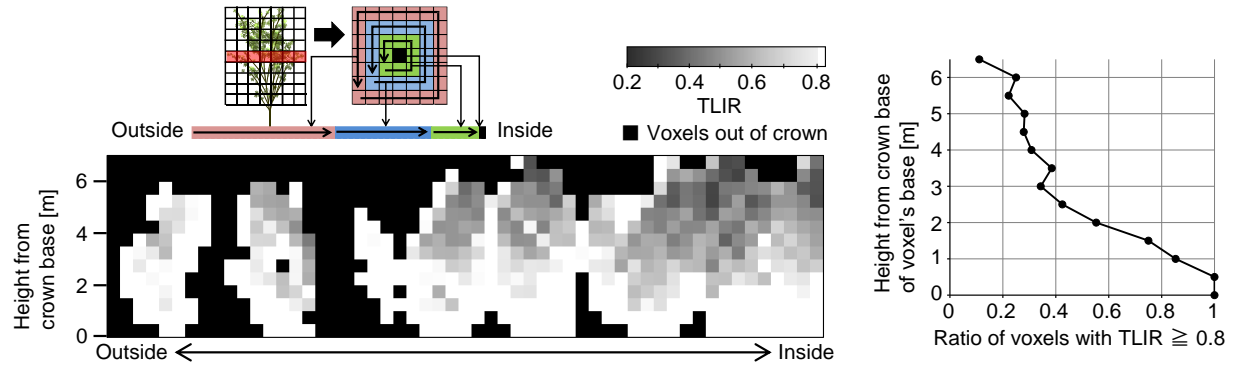


Fig. 7. Distribution of TLIR (left), variation of the ratio of voxels used in the validation ($TLIR \geq 0.8$) to all voxels at each height (right).

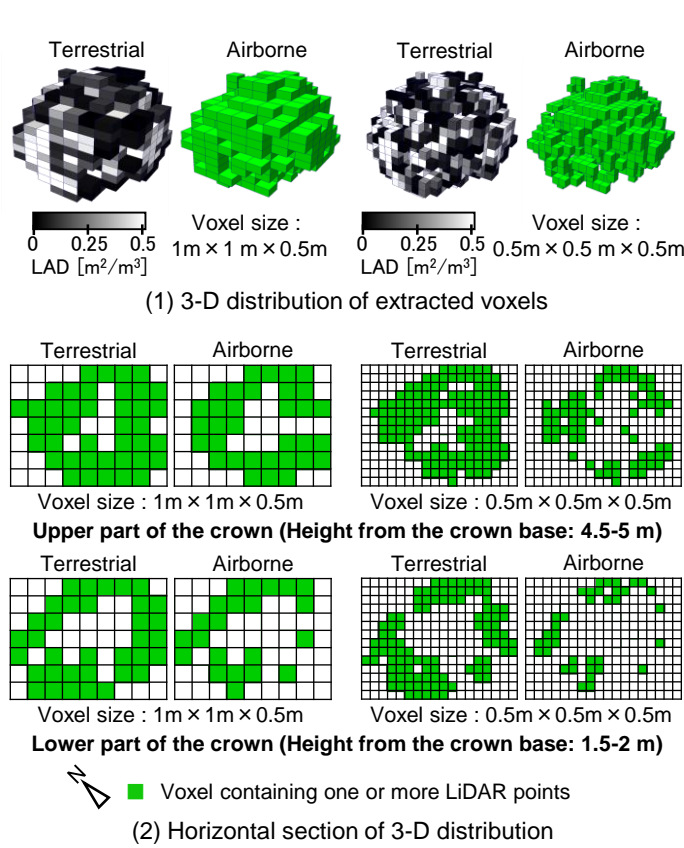


Fig. 8. Comparison between the distribution of voxels derived from airborne LiDAR and that from terrestrial LiDAR.

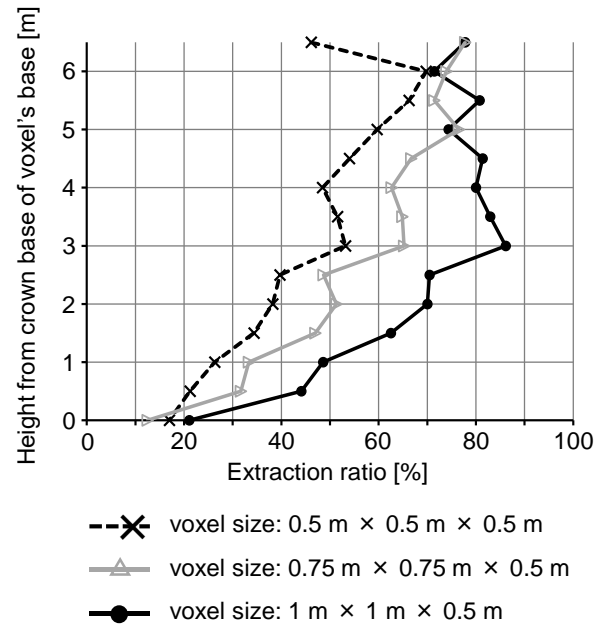


Fig. 9. Variation in the extraction ratio (ratio of voxels containing one or more airborne LiDAR points to voxels with $LAD > 0$) according to height.

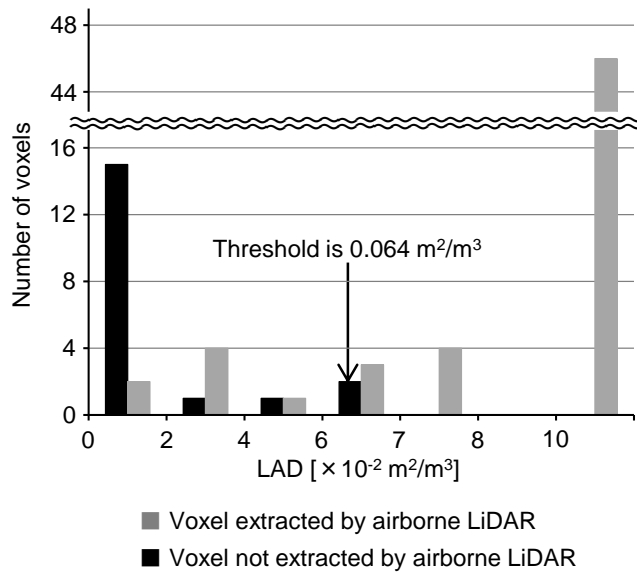


Fig. 10. Frequency distribution of terrestrial LiDAR derived-LAD for voxels extracted and not extracted by airborne LiDAR. Voxels where there are no materials between the voxel and airborne LiDAR scanner are used.

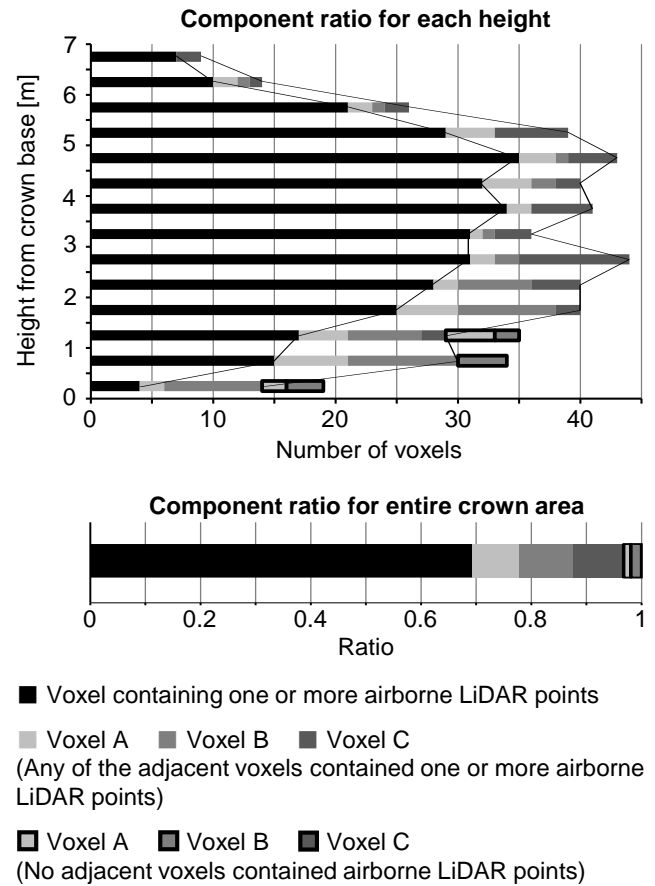


Fig. 11. Breakdown of voxels extracted by terrestrial LiDAR.

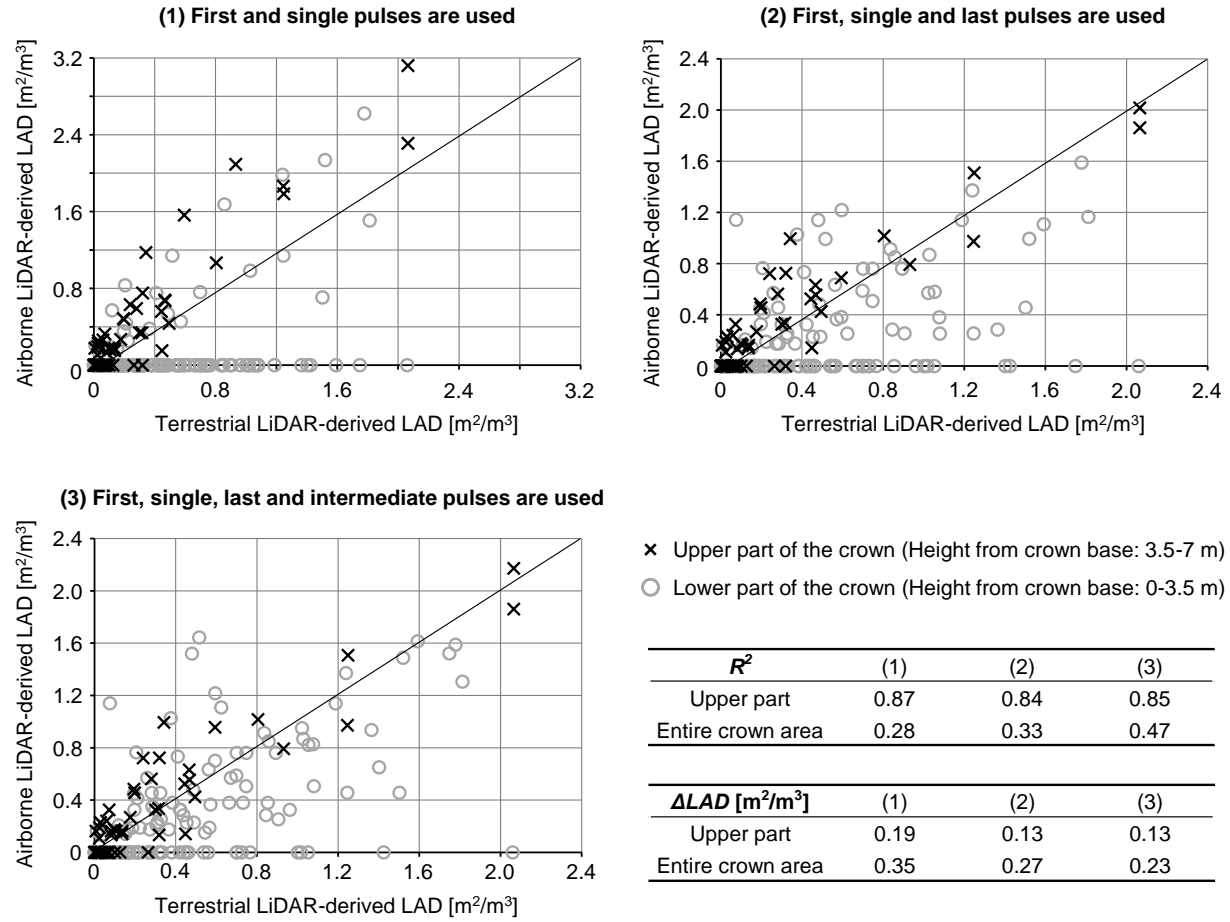


Fig. 12. Scatter plot of airborne LiDAR-derived LAD and terrestrial LiDAR-derived LAD. Each mark indicates a $1\text{ m} \times 1\text{ m} \times 0.5\text{ m}$ voxel.

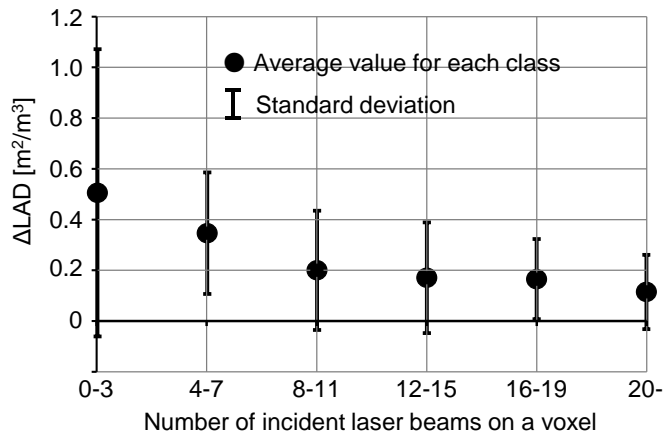


Fig. 13. Variation of ΔLAD (absolute difference between airborne LiDAR-derived LAD and terrestrial LiDAR-derived LAD) according to number of laser beams incident on a voxel.

Table 1 Airborne LiDAR observation specifications

Date: 2010.9.6	Observation system: SAKURA
Altitude: 350 m	(Heliborne system, Nakanihon Air Service)
Laser interval on the ground under the flight course: 0.25 m (scan direction), 0.2 m (flight direction)	
Scanner: LMS-Q560 (RIEGL)	Wave length: 1550 nm
Ranging accuracy: 20 mm	Laser beam divergence: 0.5 mrad
Range resolution: 0.5 m	Number of targets per pulse: unlimited

Table 2 Terrestrial LiDAR observation specifications

Date: 2010.9.2	Scanner: VZ-400 (RIEGL)
Scan angle range: -40–60° (vertical), 360° (horizontal)	
Interval between consecutive laser shots: 0.04°	
Point interval: 7 mm (vertical plane at 10 m ahead)	
Wave length: 1550 nm	Ranging accuracy: 5 mm
Laser beam divergence: 0.3 mrad	

Table 3 Extraction ratio in the entire crown area [%]

Voxel size	0.5 m	0.75 m	1 m
Ratio	44.2	55.1	69.3